Experimental Validation of a Car-Like Automated Guided Vehicle with Trajectory Tracking, Obstacle Avoidance, and Target Approach

Chih-Lyang Hwang, *Senior Member, IEEE*, and Hsing-Hao Huang
Department of Electrical Engineering, National Taiwan University of Science and Technology, Taiwan, R.O.C.

***Abstract*— The proposed hierarchical sliding mode control (HSMC) for the car-like automated guided vehicle (CLAGV) includes two parts: one is virtual control input (VCI), the other is sliding mode tracking control (SMTC) [1]. Moreover, a single software/hardware based platform develops the software for the control, image processing and trajectory planning algorithms, and the hardware for the control signal (e.g., the PWM for driving the motor) and for the sensor inputs (e.g., the decoder for obtaining the position or velocity of motor, the USB interface for capturing the image). The RGB-D vision system can detect the obstacle(s) through the depth image and recognize the specific object through the SURF (Speed-Up Robust Feature) method. The estimated distance with respect to the vehicle can execute the task of obstacle avoidance (OA) and target approach (TA). Finally, the experiments of the straight-line and circular trajectory tracking with the simultaneous OA and TA of the vehicle confirm the effectiveness, efficiency, and robustness of the proposed system.**

***Index Terms*—Automated Guided Vehicle, Hierarchical sliding mode control, Obstacle avoidance, Target approach, Software/ hardware based platform.**

I. Introduction

The rapid development of robotics technology made it possible for robots to be used for tasks requiring the cooperation with humans, e.g., health-care-related tasks, home automation, construction, surveillance, etc. In these situations, motion planning, obstacle avoidance, target approach, and trajectory tracking of automated guided vehicle (AGV) or mobile robot have become important topics ([1]-[14]). Each paper contains its own advantages and disadvantages. Most of the above papers are theoretical study and don't include an experimental validation, or don't consider different ground conditions caused by friction force and torque, or don't examine the dc motor dynamics ([2]-[10]). On the contrary, the papers [1], [11], [12] do consider different ground conditions caused by friction force and torque, and the papers [1], [13], [14] do examine the dc motor dynamics.

In this paper, not only the hierarchical principle ([1], [15]-[16]) caused by the consideration of motor dynamics for the trajectory tracking is developed but also the corresponding experimental validation is presented to confirm the consistence and effectiveness. The proposed controlled system includes the kinematic and dynamic models of a CLAGV, and the dynamic model of dc motor in the front and rear wheels. Based on the system characteristics, the direct and indirect output modes are first divided. The indirect output is the pose of the vehicle and the direct output is the motor current of the front and rear wheels. The indirect desired output (e.g., the combination of straight line(s) and circular arc(s), or circle) is on-line planned based on the assigned tasks (e.g., trajectory tracking, obstacle avoidance, target approach). Then, a virtual control input is designed by the first switching surface with the indirect dynamic tracking error, so that either asymptotic or bounded tracking of indirect desired output is achieved. Subsequently, the sliding mode tracking control (SMTC) is designed by the second switching surface using direct dynamic current tracking error, so that either asymptotic or bounded tracking of direct and indirect outputs is obtained.

Furthermore, only a RGB-D vision system (e.g., [17]-[18]) is employed to localize the obstacle(s) and to recognize the specific object. At the beginning, the obstacle is detected by the depth image and then estimated to determine that either the right- or left-hand side of the vehicle is employed to avoid the corresponding obstacle. Since the energy consumption for the straight-line trajectory of same distance is less than that for the other circular trajectories, the obstacle avoidance (OA) is designed by the trapezoid rule. Furthermore, the specific object is detected by its RGB image using Speed-Up Robust Feature (SURF) algorithm ([19]) to execute the target approach (TA) with assigned pose. Under these requirements, the functions of RGB-D vision system are fully utilized for the on-line planning trajectory required by the proposed HSMC [1], i.e., integration of VCI and SMTC. In addition, a single software/hardware based platform develops the software for the control, image processing and trajectory planning algorithms, and the hardware for the control signal (the PWM for driving the motor) and for the sensor inputs (the decoder for obtaining the position or velocity of motor, the USB interface for capturing the image) [20]. They are executed in parallel, hence are much faster ([21]). Finally, the straight-line and circular trajectory tracking with the simultaneous OA and TA validates the effectiveness, efficiency, and robustness of the proposed control system.

II. Experimental Setup and Problem Statement

A. Experimental Setup

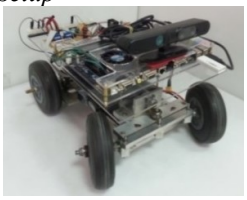

(a) Photograph.

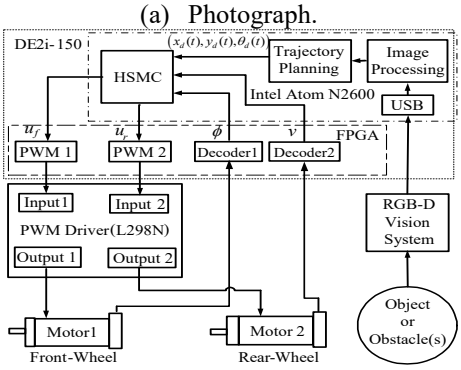

(b) Block diagram.

Fig. 1. The proposed CLAGV.

978-1-5386-1127-2/17/$31.00 ©2017 IEEE

Figure 1 shows the experimental setup of a CLAGV. The overall control system includes (i) two dc motors, (ii) one driver, (iii) one software/hardware based platform, (iv) RGB-D vision system (see Fig. 1(b)). Two dc motors are the A-max 32 model no. from Maxon Co. with gear ratios 50:1 and 30:1, respectively. The PWM driver is the model no. L298. The important specifications of DE2i-150 are as follows: (i) microprocessor: Intel® Atom™ Dual Core Processor N2600 (1M Cache, 1.6GHz); 64-bit Integrated Graphics with Base Frequency 400MHz. (ii) FPGA: 49,760 Les; 6,480 Kbits embedded memory; 8 PLLs. The control, image processing and trajectory planning algorithms are computed in the Intel® Atom N2600; the PWM for driving the motor and the decoder for obtaining motor position or velocity are executed in the FPGA; the image is captured from USB interface.

The proposed RGB-D vision system is the ASUS Xtion Pro Live with PrimeSense PS1080 architecture, using light coding and optical technologies. It is at the height of 25*cm* and possesses zero pitch angles with respect to the X-Y plane. The corresponding fields of view (FOVs) for the horizontal and vertical planes at different distances are depicted in Fig. 2. Since the obstacle(s) and object with specific widths and heights are on the ground, the suitable distance for obstacle and object detection is from 100 to 300*cm*.

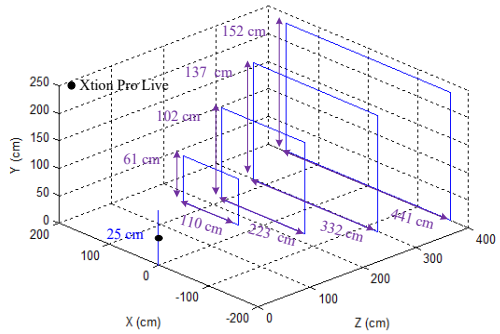

Fig. 2. FOVs of RGB-D vision system at different distances.

B. Problem Statement

Although the kinematics is based on the non-slipping condition, the friction force and torque of vehicle caused by different ground conditions must be considered to compensate the holonomic condition. However, due to their time variant feature, they are not so easy to obtain. They are assumed to be as part of the uncertainties. The dynamics of the mechanical subsystem of the dc motor is included in that of the vehicle. The dynamics of the electrical subsystem of the dc motor is dominant as high-frequency dynamics to deal with time-varying feature of ground or high-frequency desired trajectory. The uncertain control gain matrix can be thought as input disturbances, e.g., dead-zone, backlash of mechanism. In this paper, the states of indirect and direct modes are obtained from the corresponding mathematical model ($Z_1(t)$ and $Z_2(t)$ in [1]). It doesn't need an observer ([22]) such that the implementation is simplified.

The problem is to implement the control input for the CLAGV ([1]) such that the system output tracks a desired trajectory $Y_{d_1}(t)=\begin{bmatrix}x_d(t) & y_d(t) & \theta_d(t)\end{bmatrix}^T$ (see Fig. 3). First, the virtual control input $Y_{d_2}(t)=\begin{bmatrix}i_{fd}(t) & i_{rd}(t)\end{bmatrix}^T$ is designed by the first switching surface $S_1(t)$ such that the output $Y_1(t)=\begin{bmatrix}x(t) & y(t) & \theta(t)\end{bmatrix}^T$ is indirectly controlled by the output $Y_2(t)=\begin{bmatrix}i_f(t) & i_r(t)\end{bmatrix}^T$. Subsequently, the sliding mode tracking control (SMTC), i.e., $U(t)=\begin{bmatrix}u_f(t) & u_r(t)\end{bmatrix}^T$, using the second switching surface $S_2(t)$ is designed such that under suitable conditions, the $Y_2(t)$ asymptotically or boundedly tracks the virtual control input $Y_{d_2}(t)$. Since $Y_2(t)$ approaches $Y_{d_2}(t)$, this will make the indirect output $Y_1(t)$ approach $Y_{d_1}(t)$. For clearness, the control block diagram of the overall CLAGV system is depicted in Fig. 3. Finally, the experiments of trajectory tracking with concurrent obstacle avoidance and target approach by the software/hardware based platform DE2-i150 confirm the effectiveness, efficiency and robustness of the proposed control system.

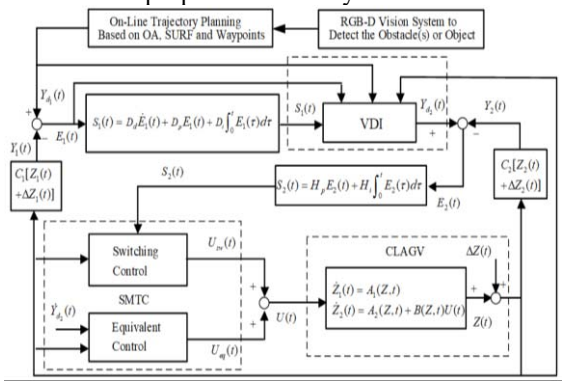

Fig. 3. Control block diagram of the overall CLAGV.

III. Strategy for Obstacle Avoidance and Target Approach, and Concept of Waypoints

A. Detection of Obstacle and Object by RGB-D Vision

In this paper, only RGB-D vision system on the vehicle is employed for the localization and recognition of the obstacle(s) and object ([17]-[19]). The accuracy of the detection using the proposed RGB-D vision system can refer to the Table 2 of the previous study [18]. At the beginning, the RGB and depth images of one obstacle are shown in Fig. 4(a), which has the resolution of 240x320 to accelerate the computation. Therefore, the pixels on the horizontal central line possess the relative depth as shown in Fig. 4(b). Then, the relation between the depth and width of the obstacle is described as follows:

$$w = 0.96d + 14(cm), \tag{1}$$

where w and d are respectively the width of the obstacle and the distance between the obstacle and the CLAGV. For instance, the depth of the obstacle in the central region, the right- and left-hand sides are approximately 1.0*m,* 3.0*m* and 5.0*m*, respectively. In this situation, the obstacle can be detected by the depth threshold 1.2*m*. In addition, the smaller width from the image center, i.e., (120,160), is assigned as the avoided side of the OA. It is known that SURF (Speed-Up Robust Feature) algorithm is robust for the feature extraction, e.g., different scales, orientations, and lighting conditions ([19]). Based on these characteristics, some recognition results are presented in Fig. 5.

The 1st column is the distance 1*m* with the front view,

rotation 30° with respect to z-axis of the RGB-D vision system, rotation 90° with respect to y-axis (or turning down), and slight darkness; the 2nd and 3rd columns are similar with the 1st column except the distances 1.5m and 2m, respectively. Due to the resolution reduction, the case of Fig. 5(i) fails since it is at 2m with rotation 45° with respect to y-axis. Thus, the distance for the object recognition is between 1m and 2m. The computation time for the SURF in DE2i-150 is around 800ms. Hence, the object recognition is only after the CLAGV reaches the target point (cf., Fig. 6).

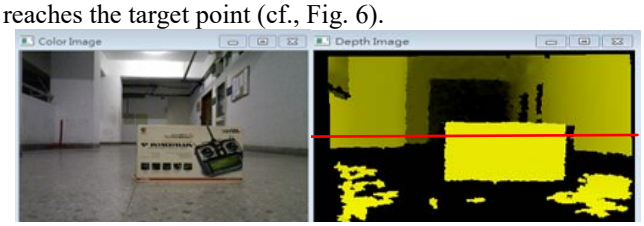

(a) RGB and depth images.

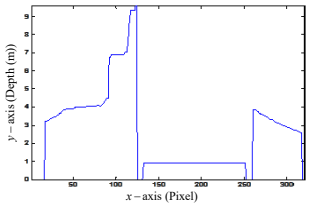

(b) Depth of the horizontal central line of the image.

Fig. 4. Image processing for the obstacle detection.

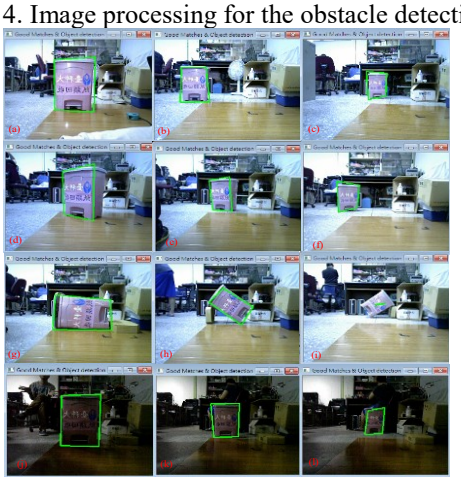

Fig. 5. Detection and recognition of an object.

B. Strategy of OA and TA by Waypoints

After the localization of obstacle, if the obstacle is on the planned trajectory, the obstacle avoidance (OA) will be executed by the threshold of depth (e.g., 1.2m). Otherwise, the CLAGV will keep tracking the trajectory until the target point is reached. The strategy of OA is designed as follows: First, the point corresponding to the smallest distance between the vehicle and the obstacle is marked as the based point (i.e., the p_b in Fig. 6). Then the vertical distances from the optical axis (or y-axis) of the vehicle are estimated by the method in Fig. 4. The symbols in Fig. 6 are illustrated as follows: (a) (x_{s0}, y_{s0}) is the start point to execute the strategy of the OA. (b) d_0 is the distance between (x_{s0}, y_{s0}) and p_b. (c) L_n and R_n are respectively the accumulated pixel numbers on the left-hand side (LHS) and right-hand side (RHS) of p_b, if the vertical distance is smaller than depth threshold, e.g., in Fig. 4(b), L_n=37, R_n =100. (d) d_m is the obstacle width for the side with the smaller pixel number, e.g., left side in Fig. 4(b). (e) d_w is the detected width of the obstacle perpendicular to the optical axis. (f) Four points (x_{s0}, y_{s0}), (x_{s1}, y_{s1}), (x_{s2}, y_{s2}), and (x_{s3}, y_{s3}) of the trapezoid are for the OA. (f) θ is the angle between the orientation of the CLAGV and the horizontal (or X-) axis of the world coordinate. Based on the OA from LHS in Fig. 6, the relations are given as follows:

$$\begin{cases} x_{s1} = x_{s0} + d_3\cos(\theta \pm \delta) \\ y_{s1} = y_{s0} + d_3\sin(\theta \pm \delta) \end{cases}, \begin{cases} x_{s2} = x_{s1} + d_4\cos(\theta) \\ y_{s2} = y_{s1} + d_4\sin(\theta) \end{cases}, \quad (2)$$
$$\begin{cases} x_{s3} = x_{s2} + d_3\cos(\theta \mp \\ y_{s3} = y_{s2} + d_3\sin(\theta \mp \end{cases}$$

where $d_1 = \gamma_1 d_0$, $d_2 = \gamma_2 d_m$, $d_3 = \sqrt{d_1^2 + d_2^2}$, $d_4 = \gamma_4 d_0$, with adjustable parameters $1 > \gamma_1 > 0$, $3 > \gamma_2 > 1$, $\gamma_u > \gamma_4 > 0$, and $\delta = \text{artan}\{d_2/d_1\}$, and $\pm$ are respectively for the OA from LHS and RHS. The parameter γ_u or γ_4 is connected with the long axis of the ellipse (or d_w). It indicates that if d_0, d_m, d_w, and θ are known, the required OA is achieved.

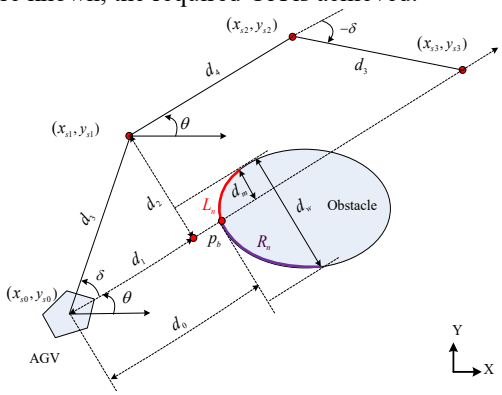

Fig. 6. Obstacle avoidance via trapezoid type.

Since the CLAGV possesses the smallest turning radius, the pose tracking (e.g., electricity charge) becomes paramount. Therefore, the target approach of the CLAGV is defined as it reaches the assigned pose with respect to the specific object. The waypoints for reaching an end point from LHS in Fig. 7 possess the following geometric relation:

$$\begin{cases} \bar{x}_{s1} = \bar{x}_{s0} + \bar{d}_2\cos(\theta \pm \bar{\delta}) \\ \bar{y}_{s1} = \bar{y}_{s0} + \bar{d}_2\sin(\theta \pm \bar{\delta}) \end{cases}, \begin{cases} \bar{x}_{s2} = \bar{x}_{s1} + \bar{d}_3\cos(\theta) \\ \bar{y}_{s2} = \bar{y}_{s1} + \bar{d}_3\sin(\theta) \end{cases}, \quad (3)$$

where $\pm$ are respectively for the LHS and RHS, θ is the angle between the orientation of the vehicle and the X-axis, $(\bar{x}_{s0}, \bar{y}_{s0})$ is the target point for searching the specific object and reaching the end point, $\bar{d}_4$ and $\bar{d}_1$ are respectively the depth and the horizontal distance between the vehicle and the object, $\bar{d}_0 = \bar{d}_4/2$, $\bar{d}_2 = \sqrt{\bar{d}_0^2 + \bar{d}_1^2}$, $\bar{d}_3 = \bar{d}_4/2 - d_d$, $d_d = 0.2m$ is the distance between an end point and the object, and $\bar{\delta} = \text{artan}\{\bar{d}_1/\bar{d}_0\}$. The purposes of waypoints are to correct the pose of the vehicle at the end point and to reduce the tracking error for the long (straight-line) desired trajectory. No pre-request information of obstacle or object is required for this study. The proposed on-line recognition and distance estimation of obstacle and object become more competitive

for practical environment.

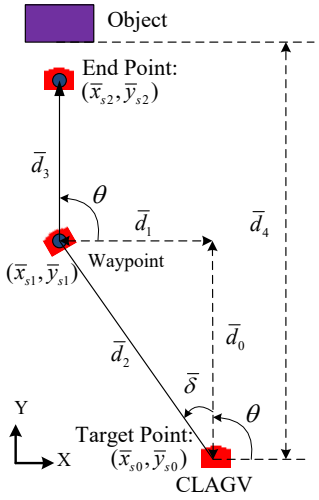

Fig. 7. Concept of waypoints.

IV. Experimental Results and Discussions

A. Experimental Results

First, the coefficients of the two switching surfaces are as follows ([1]): $D_d = diag\{64,64,20\}$, $D_p = diag\{48,36,12\}$, $D_i = diag\{0.2,0.2,0.08\}$, $H_p = I_2$, and $H_i = 1.5I_2$. The control parameters of the HSMC are assigned as follows: the boundary layer $\mu_1, \mu_2 = 0.1$, the upper bounds of uncertain control gain $\gamma_1, \gamma_2 = 0.1$, and the switching gain matrices $\Omega_{11} = diag\{84,84,42\}$, $\Omega_{12} = diag\{0.84,0.84,1.26\}$, $\Omega_{21} = 30I_2$, $\Omega_{22} = 0.75I_2$. For the practical purpose, the saturated control input is set as $10volt$. The sampling time is 0.009 second for the motion control. On the other hand, the sampling time for the image processing is 0.036 second, which is four times of the motion control.

The task 1 is assigned as follows: (i) the initial state of the CLAGV $[x(0) \quad y(0) \quad \theta(0)] = [1.5 \quad -2 \quad \pi/2]$, (ii) track a straight-line trajectory with a target point at $(x_d(t), y_d(t)) = (0,11)m$, (iii) after the reach of the target point, using SURF to recognize the object and then estimate distance between them, and (iv) command that the CLAGV reaches the end point (i.e., in front of the object by $20cm$). The response of the task 1 using the proposed HSMC is shown in Fig. 8, which contains 12 waypoints. Similarly, the response of the task 2, which is the task 1 with two static obstacles at $(x(t), y(t)) = (0.4,3)$ and $(-0.4,9)m$, is shown in Fig. 9. The experimental video can refer to the URL: https://www.youtube.com/watch?v=HqfOhG-p6t8&feature=youtu.be.

For further verification of the proposed control system, the desired circular trajectory with diameter $5m$ for the CLAGV with the initial state $[x(0) \quad y(0) \quad \theta(0)] = [0 \quad 0 \quad 0]$ is addressed. In this situation, the end point is at $(-3,-1.5)m$, the desired trajectory is assigned as $x_d(t) = 2.5\cos(\theta_d)m$, $y_d(t) = 2.5sin(\theta_d)m$, and $\theta_d(t) = 0.122t + \pi/2$. There are 6000 steps (or 54s) for a full desired circular trajectory. The corresponding response is shown in Fig. 10, which is acceptable. Similarly, the response for two static obstacles at $(x(t), y(t)) = (-1.9,-1.9)$ and $(-1.5,2)m$ with suitable sizes and respectively placed for $t \geq 30s$ and $t \geq 65s$ is shown in Fig. 11, which is also satisfactory. The corresponding experimental video is at the URL: https://www.youtube.com/watch?v=JmXv-AYvqfk&feature=youtu.be.

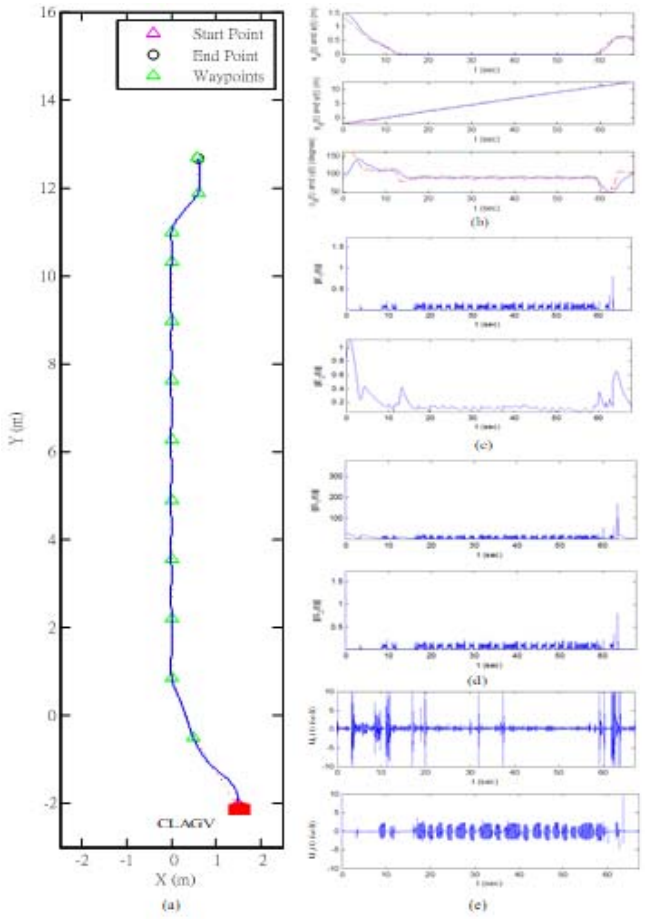

Fig. 8. Response of the CLAGV with initial pose not on the desired straight-line trajectory to approach an end point.

B. Discussions

The notations in Figs. 8(a)-11(a) have the following: $(x_d(t), y_d(t))(\cdots$ and $(x(t), y(t))(-)$. Based on these experimental results, the important observations are drawn as follows: (i) To confirm the trajectory tracking ability of the proposed HSMC, two initial poses are away from the desired trajectory before avoiding the obstacles and reaching the end point (i.e., Figs. 10 and 11). (ii) In addition, only a smaller power is required to start the vehicle as compared with the manipulation of the vehicle (cf. the transience and the time intervals for the larger control inputs in Figs. 8(e)-11(e)). (iii) Furthermore, the RGB-D vision system with the strategy of the OA, the object recognition by SURF algorithm, and the concept of waypoints accomplishes the assigned task. (iv) Due to the smallest turning radius of the CLAGV (about $0.5m$), the responses of the orientation in Figs. 9(b) and 11(b) are poorer than that in Figs. 8(b) and 10(b), which are without execution the OA. (v) From Figs. 8(e)-11(e), the saturation of the front-wheel motor more likely occurs as compared with that of the rear-wheel motor. The reasons are as follows:

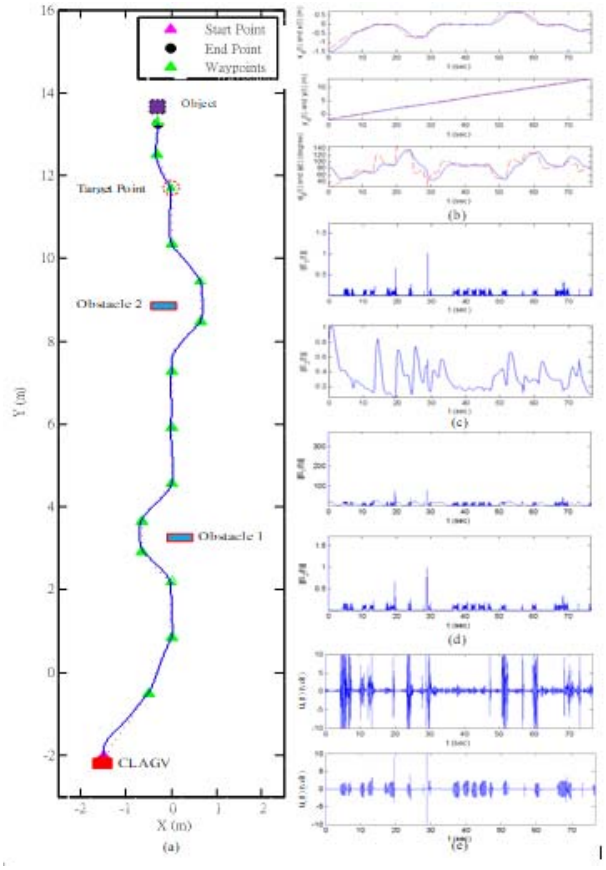

Fig. 9. Response of Figure 8 case with two obstacles.

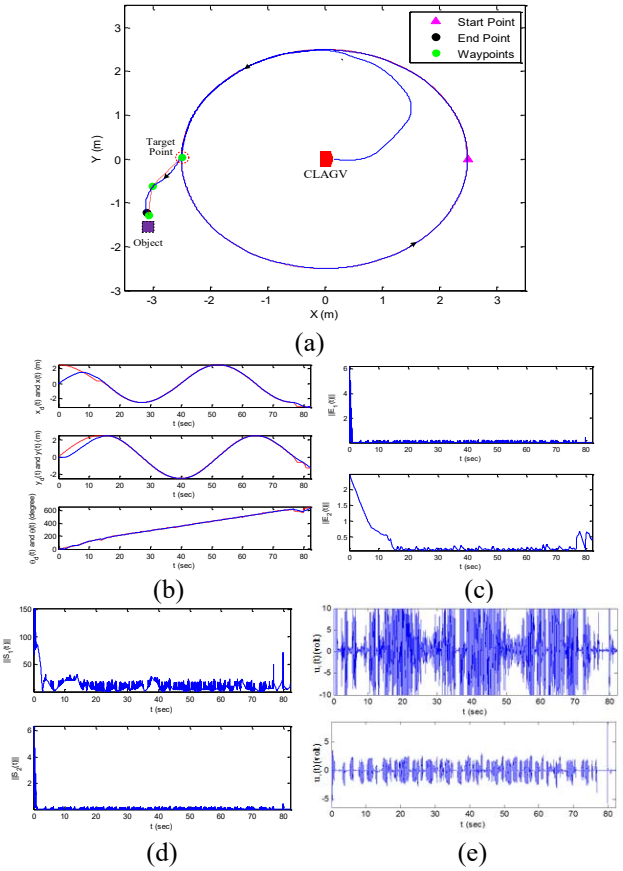

Fig. 10. Response of the CLAGV with $[x(0) \quad y(0) \quad \theta(0)] = 0$ to track a circle with diameter $5m$ without the obstacle to reach an end point.

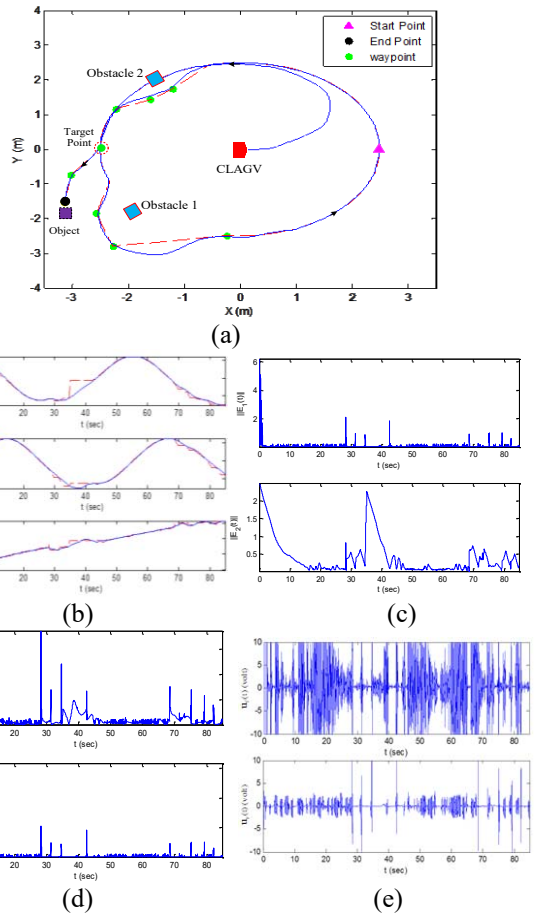

Fig. 11. Response of Figure 10 case with two obstacles.

(a) The responses of the position are smoother than that of the orientation (comparing the 1st, 2nd subplots with the 3rd subplot in Figs. 9(b) and 11(b)). (b) The high-frequency response of the front wheel with four-linkage mechanism maintains the continuous tracking ability. (c) On the other hand, the response of the rear wheel with rotary mechanism is often easier to operate. (d) The initial startup from almost zero velocity (e.g., waypoint) needs a larger peak current (or voltage) to adjust the required orientation of CLAGV. (vi) From the result of Fig. 11, the following facts are concluded. (a) The OA2 is executed by the inside of the circular trajectory; in contrast, the OA1 is executed by the outside of the circular trajectory. (b) The distance for the OA2 is smaller than that of the OA1. (c) Due to the constraint of the smallest turning radius, the OA1 can't directly avoid the obstacle 1 (cf. the 1st and 2nd subplots of Fig. 11(b)). (vii) As compared the control inputs for tracking straight-line trajectory with that for tracking circular trajectory (cf., Figs. 8(e), 10(e) and Figs. 9(e), 11(e)), the energy consumption for the same distance of the straight-line trajectory is smaller than that of the circular trajectory due to the smaller input voltages for two motors. (viii) Similarly, the responses for different initial poses or desired trajectories of Figs. 8-11 can be achieved. (ix) The proposed method can be extended to the other categories of AGV, e.g., omnidirectional type [3], differential type [23].

V. Conclusions

The model of CLAGV is hierarchical and under-actuated. For reflecting different ground conditions or the violation of non-holonomic constraint, the friction force and

torque of vehicle are also considered. The proposed hierarchical sliding mode control including SMTC and VCI [1] is designed such that the CLAGV can either asymptotically or boundedly track the desired pose of the vehicle in a robust manner. According to the detection of obstacles by depth image, the object recognition by SURF algorithm, the distance estimation by depth image, the strategy of obstacle avoidance, and the concept of waypoints, the on-line trajectory planning to accomplish the assigned tasks (trajectory tracking, obstacle avoidance, and target approach) is accomplished. Moreover, the multiple platform-based system is replaced by a single software/hardware based platform. The experiments of straight-line and circular trajectory tracking with the simultaneous OA and TA validate the effectiveness, efficiency, and robustness of the proposed control system.

References

[1] C. L. Hwang, "Comparison of path tracking control of a car-like mobile robot with and without motor dynamics," *IEEE/ASME Trans. Mechatronics*, vol. 21, no.4, pp. 1801-1811, Jun. 2016.

[2] Y. Wang, Z. Miao, H. Zhong, and Q. Pan, "Simultaneous stabilization and tracking of nonholonomic mobile robots: A Lyapunov-based approach," *IEEE Trans. Contr. Syst. Technol.,* vol. 24, no. 4, pp. 487-501, Jul. 2015.

[3] J. T. Huang, T. V. Hung, and M. L. Tseng, "Smooth switching robust adaptive control for omnidirectional mobile robots," *IEEE Trans. Contr. Syst. Technol.*, vol. 23, no. 5, pp. 1986-1994, Sep. 2015.

[4] R. de Castro, M. Tanelli, R. E. Araújo, and S. M. Savaresi, "Minimum-time path-following for highly redundant electric vehicles," *IEEE Trans. Contr. Syst. Technol.,* vol. 24, no. 2, pp. 487-501, Mar. 2016.

[5] Z. Li, C. Yang, C. Y. Su, J. Deng, and W. Zhang, "Vision-based model predictive control for steering of a nonholonomic mobile robot," *IEEE Trans. Contr. Syst. Technol.,* vol. 24, no. 2, pp. 553-563, Mar. 2016.

[6] J. Jiang, P. D. Franco, and A. Astolfi, "Shared control for the kinematic and dynamic models of a mobile robot*," IEEE Trans. Contr. Syst. Technol.,* vol. 24, no. 6, pp. 2112-2124, Nov. 2016.

[7] K. Worthmann, M. W. Mehrez, M. Zanon, G. K. I. Mann, R. G. Gosine, and M. Diehl, "Model predictive control of nonholonomic mobile robots without stabilizing constraints and costs," *IEEE Trans. Contr. Syst. Technol.,* vol. 24, no. 4, pp.1394 - 1406, Jul. 2016.

[8] W. Sun, S. Tang, H. Gao, and J. Zhao, "Two time-scale tracking control of nonholonomic wheeled mobile robots," *IEEE Trans. Contr. Syst. Technol.,* vol. 24, no. 6, pp. 2059 -2069, Nov. 2016.

[9] A. S. Matveev, M. C. Hoy, and A. V. Savkin, "Extremum seeking navigation without derivative estimation of a mobile robot in a dynamic environmental field," *IEEE Trans. Contr. Syst. Technol.,* vol. 24, no. 4, pp. 1084-1091, May 2016.

[10] B. Li, Y. Fang, G. Hu, and X. Zhang, "Model-free unified tracking and regulation visual servoing of wheeled mobile robots," *IEEE Trans. Contr. Syst. Technol.,* vol. 24, no. 4, pp. 1328-1339, Jul. 2016.

[11] R. Loureiro, S. Benmoussa, Y. Touati, R. Merzouki, and B. O. Bouamama, "Integration of fault diagnosis and fault-tolerant control for health monitoring of a class of MIMO intelligent autonomous vehicles," *IEEE Trans. Veh. Technol.*, vol. 63, no. 1, pp. 30-39, Jan. 2014.

[12] J. C. L. Barreto S., A. G. S. Conceic˜ao, C. E. T. D´orea, L. Martinez, and E. R. de Pieri, "Design and implementation of model-predictive control with friction compensation on an omnidirectional mobile robot," *IEEE/ASME Trans. Mechatronics*, vol. 19, no. 2, pp. 467-476, Apr. 2014.

[13] R. J. Wai and R. Muthusamy, "Fuzzy-neural-network inherited sliding-mode control for robot manipulator including actuator dynamics," *IEEE Trans. Neural Netw. & Learn. Syst.*, vol. 24, no. 2, pp. 274-287, Feb. 2013.

[14] H. S. Kim and J. B. Song, "Multi-DOF counter balance mechanism for a service robot arm," *IEEE/ASME Trans. Mechatronics,* vol. 19, no.6, pp. 1756-1763, Dec. 2014.

[15] C. M. Lin and Y. J. Mon, "Decoupling control by hierarchical fuzzy sliding-mode controller," *IEEE Trans. Contr. Syst. Technol*., vol. 13, no. 4, pp. 593-598, Jul. 2005.

[16] C. L. Hwang, C. C. Chiang, and Y. W. Yeh, "Adaptive fuzzy hierarchical sliding-mode control for the trajectory tracking of uncertain under-actuated nonlinear dynamic systems," *IEEE Trans. Fuzzy Syst.,* vol. 22, no. 2, pp. 286-297, Apr. 2014.

[17] E. Ohn-Bar and M. M. Trivedi, "Hand gesture recognition in real time for automotive interfaces: A multimodal vision-based approach and evaluations," *IEEE Trans. Intell. Trans. Syst.*, vol. 15, no. 6, pp. 2368-2377, Dec. 2014.

[18] C. L. Hwang, B. L. Chen, H. H. Huang, and H. T. Syu, "Hybrid learning model and MMSVM classification for on-line visual imitation of a human with 3-D motions," *Robotics and Autonomous Systems*, vol. 71, pp. 150-165, 2015.

[19] J. W. Hsieh, L. C. Chen, and D. Y. Chen, "Symmetrical SURF and its applications to vehicle detection and vehicle make and model recognition," *IEEE Trans. Intell. Transp. Syst.,* vol. 15, no. 1, pp. 6-20, Feb. 2014.

[20] J. Rodríguez-Araújo, J. J. Rodríguez-Andina, J. Fariña, and M. Y. Chow, "Field-programmable system-on -chip for localization of UGVs in an indoor iSpace," *IEEE Trans. Ind. Inform.*, vol. 10, no. 2, pp. 1033- 1043, May 2014.

[21] Z. Hajduk, B. Trybus, and J. Sadolewski, "Architecture of FPGA embedded multiprocessor programmable controller," *IEEE Trans. Ind. Electron.*, vol. 62, no. 5, pp. 6952-6961, May 2015.

[22] C. L. Hwang, Y. M. Chen and C. Jan, "Trajectory tracking of large-displacement piezoelectric actuators using a nonlinear observer-based variable structure control," *IEEE Trans. Control Syst. Technol.*, vol. 13, no. 1, pp.56-66, Jan. 2005.

[23] C. L. Hwang, C. C. Yang, and J. Y. Hung, "Path tracking of an autonomous ground vehicle with different payloads and ground conditions by hierarchical improved fuzzy dynamic sliding-mode control," *IEEE Trans. Fuzzy Syst.*, to appear, 2017.